

# Communication-Free Power Management Strategy for the Multiple DAB-Based Energy Storage System in Islanded DC Microgrid

Nie Hou<sup>1</sup>, Student Member, IEEE, and Yunwei Li<sup>1</sup>, Fellow, IEEE

**Abstract**—Along with the development of the renewable energy, such as the photovoltaics and the wind turbine, the energy storage system (ESS) is becoming as a critical part for the renewable-based microgrids. In this article, dual-active-bridge (DAB) dc–dc converter with bidirectional power flowing ability, wide soft-switching range, and ultrafast dynamic characteristic is adopted for integrating multiple energy storage units (ESUs) for balancing the power flowing between the renewable energy and the loads in a islanded dc microgrids. For the multiple DAB-based ESS, a communication-free power management strategy is proposed in this article to maintain the dc-link voltage for the islanded dc microgrid, and high robustness of the dc-link voltage can be ensured when the output voltage of energy storage equipment, the load condition, and the power sharing performance of the ESS are changed. The proposed strategy also ensures seamless ESU plug-in or plug-out operations. Finally, the small-scale simulation model and experimental platform are both employed to verify the effectiveness of the proposed communication-free power management scheme.

**Index Terms**—Energy storage system (ESS), hot swap, islanded dc microgrid, power sharing control.

## I. INTRODUCTION

**I**N RECENT years, there is a rapid development of renewable energy system, such as photovoltaics, wind turbine energy, and fuel cell, to reduce the reliance on fossil fuels [1]–[5]. Since these power sources are usually generated as dc power before transmission, dc microgrids are currently considered to be an efficient method for integrating distributed renewable resources with less power conversion stages and without traditional issues, such as harmonics, synchronization, and unbalance [6]–[8].

To guarantee the reliable operation and power quality of the microgrid, it is important to mitigate the power fluctuation caused by these renewable energy sources and provide a stable dc-bus voltage. Therefore, the energy storage system (ESS) is usually an indispensable part of the dc microgrid to balance the

Manuscript received February 20, 2020; revised May 19, 2020 and July 25, 2020; accepted August 17, 2020. Date of publication August 26, 2020; date of current version November 20, 2020. This work was supported by the Future Energy Systems Research initiative by Canada First Research Excellence Fund and Alberta Innovates. Recommended for publication by Associate Editor A. Davoudi. (*Corresponding author: Nie Hou.*)

The authors are with the Department of Electrical and Computer Engineering, University of Alberta, Edmonton, AB T6G 2V4, Canada (e-mail: nhou@ualberta.ca; yunwei.li@ualberta.ca).

Color versions of one or more of the figures in this article are available online at <https://ieeexplore.ieee.org>.

Digital Object Identifier 10.1109/TPEL.2020.3019761

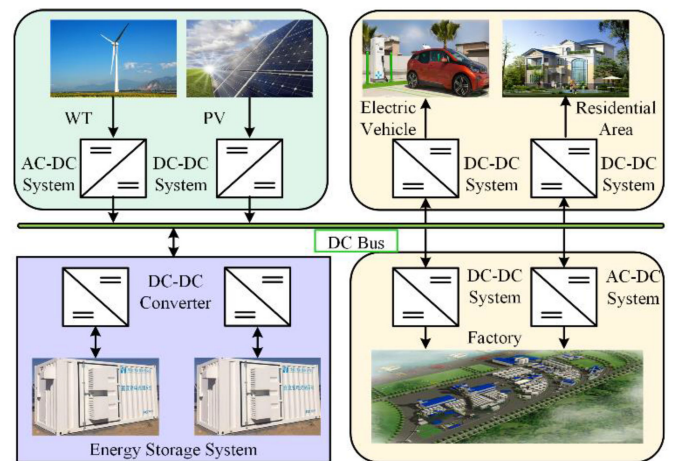


Fig. 1. Isolated microgrid with the ESS established by multiple ESUs.

power flowing between the renewable energy source and the load system [9]–[12]. The typical configuration of the dc microgrid with ESS can be shown in Fig. 1, where the ESS is usually based on multiple energy storage units (ESUs) [11]–[14]. For the ESS, there are always two main objectives, including maintaining the dc-bus voltage and configuring the power sharing performance of different ESUs.

In the islanded dc microgrid with ESS, most research focus on the traditional dc–dc converters, such as buck and boost converters, for realizing the bidirectional power transmission between dc grid bus and ESS and maintaining the dc grid voltage under different transient conditions [15]–[17]. However, these traditional dc–dc converters cannot provide electric isolation. Currently, the dual-active-bridge (DAB) dc–dc converter with the symmetric, isolated, and bidirectional characteristics becomes as a promising candidate for the dc power system, as shown in Fig. 2 [18]–[20], which can form cascading or paralleling configurations for different voltage-level requirements. Since the soft-switching performance can also be easily implemented, the high efficiency and high-power density are the advantages of this converter. Moreover, the ultrafast dynamic performance under input-voltage or load disturbances of DAB dc–dc converter can be very easily achieved, which can boost the robustness of the dc microgrid [21]–[23].

The multiple DAB-based ESS can be shown in Fig. 3, where ESUs are paralleled by using the DAB dc–dc modules. For the

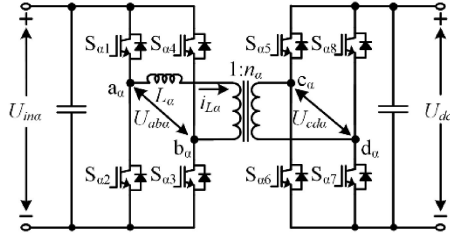


Fig. 2. Topology of the DAB dc-dc converter.

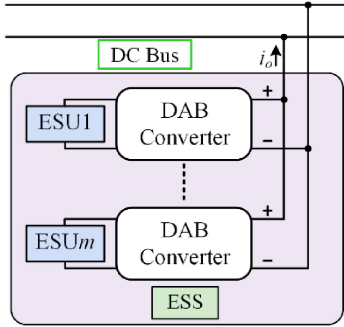


Fig. 3. Diagram of the multiple DAB-based ESS.

parallel DAB dc–dc converter system, centralized optimized dynamic control strategies with one centralized PI controller have been proposed [24]–[26], where the fast-dynamic performance can be provided for ensuring a strong dc-bus voltage. However, when a new ESU should be plugged-in for extending the power capacity of the ESS, the reprogramming operation is unavoidable with one centralized PI control structure, which is not suitable for the islanded dc microgrid. For this condition, the droop control concept may be a promising candidate. When the steady-state condition of the isolated microgrid system is achieved, the power sharing performance of the ESS can be determined by the droop coefficients [27]–[28]. Sometimes, the power sharing performance under droop concept is degraded by the line impedance, since the measured dc bus voltages for different ESU may be different caused by the line impedance. Therefore, an accurate power sharing control method is proposed to reduce the impact of the line resistance by adding the line resistor in the droop control structure [29]. Nevertheless, the accurate line resistors may be difficultly obtained in practical application, and these line resistors are changed with the temperature and the network structure of the power system. Furthermore, an improved droop control method with low bandwidth communication is proposed to detect the actual output voltage of each energy storage module and adjust the droop coefficient for accuracy current sharing performance [30]. Then, when the centralized ESS is adopted, the line impedance can be neglectful, and with suitable droop coefficients, the accurate power sharing performance among different ESUs can be acquired.

Therefore, based on the droop concept, a communication-free power management strategy is proposed for increasing the robustness of the dc-link voltage when the input voltage of the ESU, the load condition, and the power sharing performance of the ESS are changed. Moreover, the hot plug-in/out operation

without influence on the dc-link voltage is proposed. In addition, based on this proposed scheme, each ESU can not only work independently but also easily to connect with high-level management system for better control feature of state-of-charge (SOC) and centralized man-machine interaction. In the following sections, the communication-free power management strategy is proposed for the multiple DAB-based dc–dc converter system, and the design principle of the control parameters is illustrated in Section II. Moreover, the hot swap operation for the ESU is proposed and analyzed, and the potential extension to high-level control system of the proposed scheme is also illustrated. Finally, the simulation and experimental results are provided to validate the effectiveness of the presented strategies in Section III. Finally, Section IV concludes the article.

## II. COMMUNICATION-FREE POWER MANAGEMENT STRATEGY FOR THE MULTIPLE DAB-BASED ESS

In this section, for the multiple DAB-based ESS, the communication-free power management strategy is proposed to maintain the dc-link voltage when the input voltage, the load condition, and the power sharing performance of the ESS are varied. Moreover, the parameter design principle is presented. Furthermore, the seamless hot swap operation of the ESU is proposed. In addition, the potential extension to low-bandwidth high-level control system of the proposed strategy is presented.

### A. Proposed Communication-Free Power Management Strategy for the DAB-Based ESS

In order to realize the flexible power transmission, the single-phase-shift (SPS) modulation method is the most popular modulation method for the DAB dc–dc converter. Thus, in this article, the SPS modulation method is adopted, which can be illustrated in Fig. 4, where  $S_{\alpha 1}$ – $S_{\alpha 8}$  are the switching signals for the corresponding switches,  $U_{ab\alpha}$  is the output voltage of the primary-side H bridge,  $U_{cd\alpha}$  is the output voltage of the secondary-side H bridge,  $i_{L\alpha}$  is the inductance current,  $D_\alpha$  is the phase-shift ratio, and  $T_{s\alpha}$  is the switching period of the  $\alpha$ th DAB dc–dc converter for the  $\alpha$ th ESU.

When the ESU injects power to the dc grid, the transferred power of the DAB module is assumed as positive, and when the ESU absorbs power from the dc grid, the transferred power of the DAB module is assumed as negative. According to Fig. 4, the transferred power under SPS modulation method can be expressed as

$$P_\alpha = \begin{cases} l \frac{U_{in\alpha} U_{dc} D_\alpha (1-D_\alpha) T_{s\alpha}}{2n_\alpha L_\alpha} & (P_\alpha \geq 0) \\ l - \frac{U_{in\alpha} U_{dc} D_\alpha (1-D_\alpha) T_{s\alpha}}{2n_\alpha L_\alpha} & (P_\alpha < 0). \end{cases} \quad (1)$$

Then, according to (1), the phase-shift ratio  $D_\alpha$  can be calculated as

$$D_\alpha = \begin{cases} \frac{1}{2} - \sqrt{1 - \frac{8L_\alpha P_\alpha}{n_\alpha U_{in\alpha} U_{dc} T_{s\alpha}}} & (P_\alpha \geq 0) \\ \frac{1}{2} - \sqrt{1 + \frac{8n_\alpha L_\alpha P_\alpha}{U_{in\alpha} U_{dc} T_{s\alpha}}} & (P_\alpha < 0). \end{cases} \quad (2)$$

Moreover, to implement the communication-free control performance, the droop control concept is adopted in this article, and

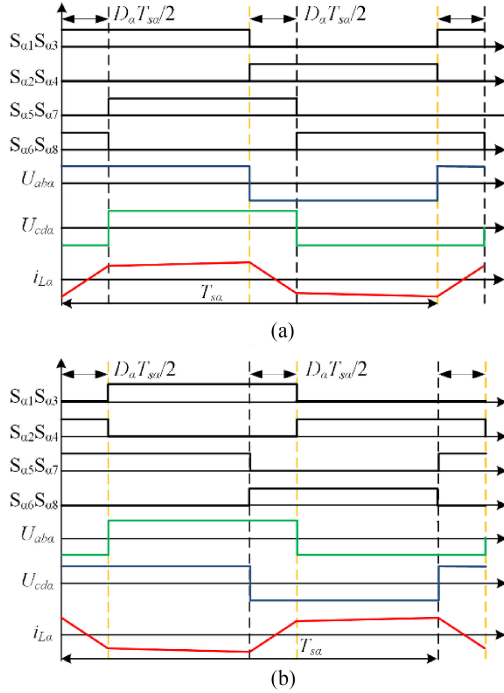


Fig. 4. SPS modulation method of DAB converter for bidirectional power flowing conditions. (a) ESUs inject power to the grid. (b) ESUs absorb power from the grid.

the desired dc-link voltage  $U_{dc\alpha}$  for each EUS can be expressed as

$$U_{dc\alpha} = U_{nom} - \frac{P_\alpha}{k_\alpha P_T^*} = U_{nom} - \frac{P_\alpha}{k_\alpha U_{nom} i_o^*} \quad (3)$$

where  $k_\alpha$  is the droop coefficient,  $U_{nom}$  is the nominal voltage of the dc grid,  $P_T^*$  is the total desired output power, and  $i_o^*$  is the desired output current of the ESS. In (3), the total desired output power  $P_T^*$  is employed to unify the transferred power  $P_\alpha$  of the  $\alpha$ th ESU, and the desired output current  $i_o^*$  of the ESS can be expressed as

$$i_o^* = \frac{U_{nom}}{R_{TE}} = \frac{U_{nom} i_o}{U_{dc}} \quad (4)$$

where  $R_{TE}$  is the total equivalent load resistor. In addition, based on the power control concept, the required transferred power for the  $\alpha$ th DAB module can be shown as

$$P_\alpha^* = \frac{U_{v\alpha} U_{nom} i_o}{U_{dc}} \quad (5)$$

where  $U_{v\alpha}$  is named as the virtual dc-link voltage, which is the output value of the outer-loop PI controller. Combining (1)–(5) and Fig. 4, the communication-free power management scheme can be illustrated as Fig. 5.

In Fig. 5, the proposed communication-free power management strategy can be realized for the multiple DAB-based ESS. For each ESU, the output current  $i_o$ , the output voltage  $U_{in\alpha}$  of the energy storage component, and the dc-link voltage  $U_{dc}$  are measured at the beginning of each switching period. Then, based on (4), the desired output current  $i_o^*$  of the ESS is calculated, and based on (1), the transferred power of each ESU can be obtained. Since the load current is adopted, the excellent dynamic

response can be obtained by using the power-based control in this proposed communication-free power management strategy. Furthermore, combining (3), the desired dc-link voltage  $U_{dc\alpha}$  for each ESU can be obtained. Moreover, based on the power control concept, the required transferred power  $P_\alpha^*$  for each ESU can be acquired by (5). In addition, combining Fig. 4 and (2), the phase-shift ratio  $D_\alpha$  can be calculated for realizing the required transferred power for each ESU. Since the input voltage is acted as the feedback value for each modulation structure, the required transferred power from the power-based control can be ensured even when the input voltage of DAB module is changed. Then, the fast-dynamic performance can be achieved when the output voltage of energy storage component is changed. Importantly, in the modulation part, other phase-shift modulation methods, such as the dual-phase-shift modulation method [31], the extended-phase-shift modulation method [32]–[33], and the triple-phase-shift modulation method [34], [35], can be employed for boosting the efficiency of the whole converter system since the transferred power is acted as the middle control value between the power-based control structure and the modulation structure [20].

Therefore, based on the proposed communication-free power management strategy for ESS, the ultrafast dynamic response can be obtained to ensure the stability of the dc system. In addition, since the control loop for each ESU contains the PI controller based on the droop control concept, which can boost the autonomy characteristic of the ESU, and it is easy to realize the hot swap of the ESU. In addition, according to (3), when the droop parameter of one ESU is reduced for smaller transferred power, other ESUs will share more power requirement with the same droop parameters, so the steady-state dc-link voltage will be close to the nominal dc-link voltage. Conversely, the steady-state dc-link voltage will be away from the nominal dc-link voltage.

### B. Design Principle of the PI Parameter and the Droop Coefficients

For DAB dc–dc converter, the relationship between the phase-shift ratio and the transferred power or current is similar in steady-state condition or during transient process [20]. Thus, leakage inductances of these converters do not affect the dynamic performance, and DAB modules can be directly regarded as current sources. Then, multiple DAB-based ESS can be simplified as Fig. 6.

Generally, when input voltage or load condition is changed, desired voltages  $U_{dc\alpha}$  from the droop control structure can be treated as constant values. Then, the power-based control method for the multiple DAB-based ESS can be illustrated in Fig. 7. Assuming ESUs are working on power balancing performance, the transfer function of each DAB module can be expressed as

$$\begin{aligned} H_\alpha(s) &= \frac{U_{nom} i_o}{m U_{dc}^2} \frac{k_{p\alpha} s + k_{i\alpha}}{s} \frac{1}{SC_{dc}} \\ &\approx \frac{i_o}{m U_{dc}} \frac{k_{p\alpha} s + k_{i\alpha}}{s} \frac{1}{SC_{dc}} \end{aligned} \quad (6)$$

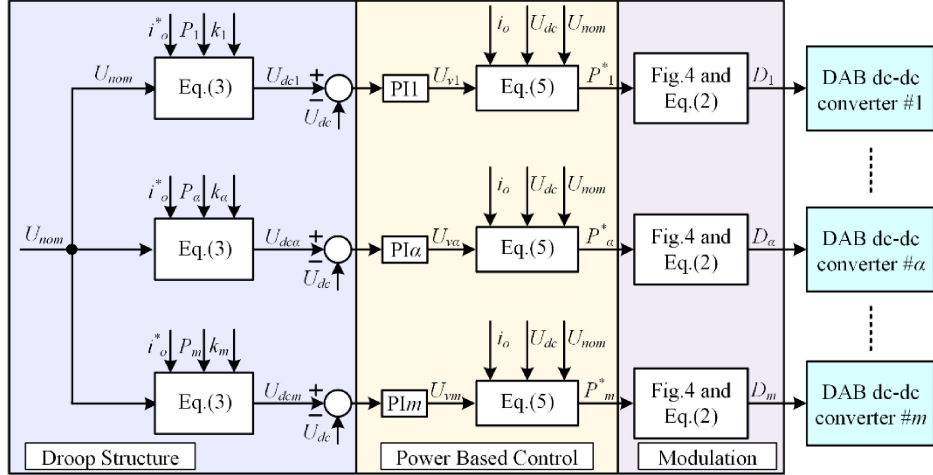


Fig. 5. Communication-free power management strategy for multiple DAB-based ESS.

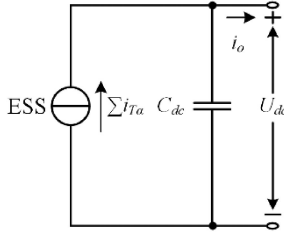


Fig. 6. Simplified circuit of multiple DAB-based ESS.

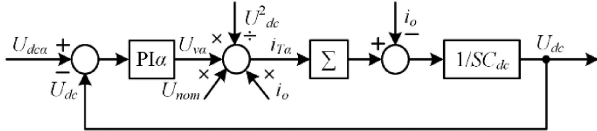


Fig. 7. Power-based control scheme for the DAB dc-dc converter.

where  $m$  is the number of the ESU,  $k_{p\alpha}$  is the proportionality coefficient, and  $k_{i\alpha}$  is the integral coefficient of the PI controller. According to (6), since DAB dc-dc converter is the first-order system with capacitive character, the phase margin always close to  $90^\circ$ . Then, in order to ensure the stability of DAB module, the crossover frequency is set as the switching frequency  $f_{s\alpha}$ . Moreover, assuming  $k_{p\alpha}$  is ten times as  $k_{i\alpha}$ ,  $k_{p\alpha}$  can be calculated as

$$k_{p\alpha} = \frac{2\pi f_{s\alpha} C_{dc} m U_{dc}}{i_o} = 2\pi f_{s\alpha} C_{dc} m R_{TE}. \quad (7)$$

Assuming the switching frequency is 10 kHz, the Bode diagram can be demonstrated as Fig. 8.

Based on (7),  $k_{p\alpha}$  is usually bigger than 100, and combining Fig. 8, the control system can provide a stable dc-link voltage. However, although oscillations of the dc-link voltage  $U_{dc}$  can be easily evitable with the dc-link capacitor, there are obvious disturbances in phase-shift ratio with measurement noise since the power transferring range of DAB converter is limited [20]. Thus, the disturbances  $\Delta D_\alpha$  of the phase-shift ratio caused by

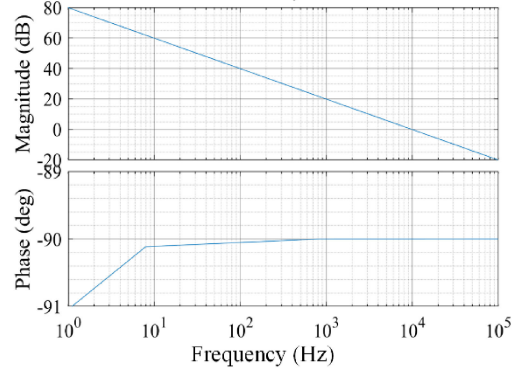


Fig. 8. Bode diagram of the power-based control method for the DAB module.

the measurement noises should also be treated as a criterion to evaluate the stability of the DAB dc-dc converter. Then, combining (2), (5), and Fig. 5, and assuming the measurement noise  $U_{dc,mn}$  and the difference of the measurement noises between two successive switching periods are close, the phase-shift ratio disturbances  $\Delta D_\alpha$  can be expressed as

$$\Delta D_\alpha \approx \sqrt{1 - \frac{8n_\alpha L_\alpha [U_{\alpha v} + (k_{p\alpha} + k_{i\alpha}) U_{dc,mn}] U_{nom} i_o}{U_{in\alpha} U_{dc}^2 T_{as}}} - \sqrt{1 - \frac{8n_\alpha L_\alpha U_{\alpha v} U_{nom} i_o}{U_{in\alpha} U_{dc}^2 T_{as}}}. \quad (8)$$

According to (8) and ignoring the higher minimum term, PI parameters can be expressed as

$$(k_{p\alpha} + k_{i\alpha})$$

$$\approx \left| \frac{\Delta D_\alpha}{U_{dc,mn}} \sqrt{1 - \frac{8n_\alpha L_\alpha U_{\alpha v} U_{nom} i_o}{U_{in\alpha} U_{dc}^2 T_{as}}} \frac{U_{in\alpha} U_{dc}^2 T_{as}}{4 U_{nom} i_o n_\alpha L_\alpha} \right|. \quad (9)$$

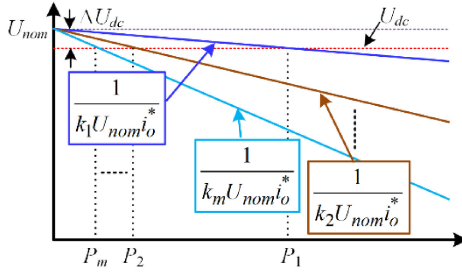


Fig. 9. Regulation characteristic of the droop control in the communication-free power management strategy.

Furthermore, assuming the maximum phase-shift ratio disturbance is  $\Delta D_{\alpha \max}$ , (9) can also be expressed as

$$(k_{p\alpha} + k_{i\alpha}) \leq \left| \frac{\Delta D_{\alpha \max}}{U_{dcmn}} \sqrt{1 - \frac{8n_\alpha L_\alpha U_{\alpha v} U_{nom} i_o}{U_{in\alpha} U_{dc}^2 T_{as}}} \frac{U_{in\alpha} U_{dc}^2 T_{as}}{4U_{nom} i_o n_\alpha L_\alpha} \right|. \quad (10)$$

Then,  $k_{i\alpha}$  can be designed as tenth of  $k_{p\alpha}$  since transferred power in steady-state condition is mainly depended on the feedback values, and (10) can be further expressed as

$$\begin{cases} k_{p\alpha} \leq \left| \frac{\Delta D_{\alpha \max}}{U_{dcmn}} \sqrt{1 - \frac{8n_\alpha L_\alpha U_{\alpha v} U_{nom} i_o}{U_{in\alpha} U_{dc}^2 T_{as}}} \frac{U_{in\alpha} U_{dc}^2 T_{as}}{4U_{nom} i_o n_\alpha L_\alpha} \right| \\ k_{i\alpha} \leq \left| \frac{\Delta D_{\alpha \max}}{10U_{dcmn}} \sqrt{1 - \frac{8n_\alpha L_\alpha U_{\alpha v} U_{nom} i_o}{U_{in\alpha} U_{dc}^2 T_{as}}} \frac{U_{in\alpha} U_{dc}^2 T_{as}}{4U_{nom} i_o n_\alpha L_\alpha} \right|. \end{cases} \quad (11)$$

In addition, the droop coefficient  $k_\alpha$  is also the main control parameter in the communication-free power management strategy for power sharing performance of different ESUs. Based on the droop control concept, the voltage error  $\Delta U_{dc}$  between the steady-state dc-link voltage  $U_{dc}$  and the nominal dc-link voltage  $U_{nom}$  in the communication-free power management system can be shown in Fig. 9. Moreover, according to (3), the voltage error  $\Delta U_{dc}$  can be expressed as

$$\Delta U_{dc} = U_{nom} - U_{dc} = \frac{P_\alpha}{k_\alpha U_{nom} i_o^*}. \quad (12)$$

When the power balancing performance is realized among different ESUs for the ESS, (12) can be further illustrated as

$$\Delta U_{dc} = \frac{1}{k_\alpha m}. \quad (13)$$

Then, assuming the allowed maximum voltage error is  $\Delta U_{dc\max}$ , the droop coefficient  $k_\alpha$  can be further expressed as

$$k_\alpha \geq \frac{1}{m \Delta U_{dc\max}}. \quad (14)$$

Notably, the allowed maximum voltage error  $\Delta U_{dc\max}$  between the nominal dc-link voltage and the steady dc-link voltage should be bigger than the measurement noise  $U_{dcmn}$ . Then, the droop coefficient  $k_\alpha$  can be further expressed as

$$\frac{1}{m \Delta U_{dc\max}} \leq k_\alpha < \frac{1}{m U_{dcmn}}. \quad (15)$$

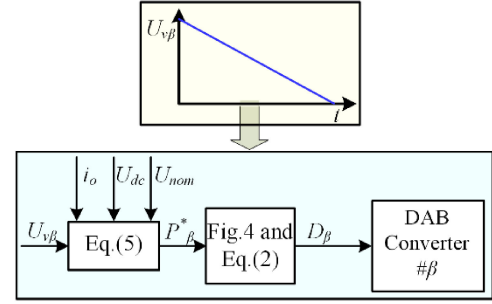


Fig. 10. Plug-out process of the  $\beta$ th DAB-based ESU.

Usually, in order to reduce the impact of the measurement noise obvious, (15) can be further expressed for the practice application as

$$\frac{1}{m \Delta U_{dc\max}} \leq k_\alpha \leq \frac{1}{2m U_{dcmn}}. \quad (16)$$

### C. Plug-In or Plug-Out Processes of the ESU

The plug-in or plug-out operations of the ESU are required for repairing the energy storage equipment and extending the power capacity for the ESS. Based on this proposed communication-free power management strategy, the new ESU can be easily plugged-in with only small influence on the dc-link voltage since the PI controller can provide a buffer function. Then, the transferred power of the new plugged-in ESU can be increased slowly, and based on the adjusting function of the PI controller and droop controller in other ESUs, the steady-state condition of the ESS can be obtained when the new ESU is completely plugged-in. According to (13), when the number of the ESUs is increased, the steady-state dc-link voltage will be a little close to the nominal dc-link voltage, and the voltage error is preferred to be smaller. Thus, when the steady-state condition is obtained again, the actual dc-link voltage will be closer to the nominal dc-link voltage.

In addition, when the  $\beta$ th DAB-based ESU should be unplugged-out, the transferred power of this ESU should become zero first, and the plug-out process of this DAB-based ESU can be shown in Fig. 10, where the virtual output voltage  $U_{v\beta}$  is gradually reduced to zero, and the transferred power of this ESU will be decreased to zero. Notably, this unplugged-out ESU can be treated as load by other ESUs, and the  $\beta$ th DAB-based ESU will not control the dc-link voltage actively. Moreover, with the feedback value of the load current and the input voltage, this unplugged-out ESU can offer the timely response when the load condition or input voltage are changed. Thus, the robustness of the dc-link voltage can be ensured during the plug-out process of the ESU. Then, when the transferred power of the  $\beta$ th DAB-based ESU becomes zero, the storage energy in the leakage inductance of the transformer should be consumed before plug-out action, and with the parallel diodes, these storage energies can transfer to the ESU and the dc-link bus by turning OFF all the switches. The corresponding circuit can be shown as Fig. 11. Furthermore, when the inductance current becomes zero, there is no

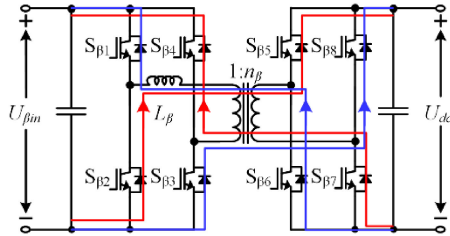


Fig. 11. Circuit condition for consuming the storage energies in the inductances of the DAB dc–dc module.

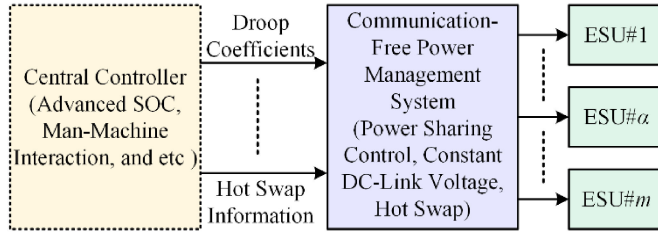


Fig. 12. Potential system structure for the proposed communication-free power management strategy with low-bandwidth high-level central controller.

exchanging power between the ESU and the dc-link bus and flowing current in DAB dc–dc module, and the  $\beta$ th DAB-based ESU can be completely plugged-out from the ESS. According to (13), when the number of the ESUs is decreased, the voltage error between the actual dc-link voltage and the nominal voltage is preferred to be bigger. Thus, when the steady-state condition is obtained again, the actual dc-link voltage will be a little away from the nominal dc-link voltage in the isolated dc microgrid.

#### D. Potential Extension to Low-Bandwidth High-Level Control System of the Proposed Communication-Free Power Management Strategy

By presetting different droop coefficients for different SOC conditions of the energy storage equipment, the balanced SOC performance among different ESUs can be obtained through relatively long-time fuzzy regulation function [36], [37]. However, sometimes, higher requirement of the SOC performance of the ESUs should be provided, and the centralized man-machine interaction system of the ESS may be required. Then, a high-level control system may be required, and the potential system structure for the communication-free power management strategy with high-level central controller can be shown in Fig. 12.

In Fig. 12, the central controller can be employed to ensure advanced SOC of different ESUs and provide good man–machine interaction system of the whole ESS. Importantly, based on the proposed communication-free power management strategy, the high-level central control system will not affect the dc-link voltage, and when the ESU is plugged-in or plugged-out, the reprogramming operation is not required since each ESU has self-regulating ability with the integrated closed-loop structure containing the independent PI controller for adjusting the dc-link voltage.

TABLE I  
CIRCUIT PARAMETERS OF THE MULTIPLE DAB-BASED DC-DC CONVERTER SYSTEM IN SIMULATION MODEL

|                             |                                     |
|-----------------------------|-------------------------------------|
| Number of DAB Modules       | 3                                   |
| $L_1, L_2, L_3$             | 50 $\mu$ H, 80 $\mu$ H, 100 $\mu$ H |
| $n_1, n_2, n_3$             | 2                                   |
| $f_s$                       | 10kHz                               |
| $R_{TE}$                    | 10 $\Omega$ or 30 $\Omega$          |
| $U_{in1}, U_{in2}, U_{in3}$ | 50V to 60V                          |
| $U_{nom}$                   | 100.66V (Compensated)               |
| $U_{dc}^*$                  | 100V                                |
| $k_1, k_2, k_3$             | 0 to 1                              |
| $k_{pas}, k_{ia}$           | 2.5, 0.25                           |

### III. SIMULATION AND EXPERIMENT VERIFICATIONS

In this section, based on Simulink model and experiment platform of the multiple DAB-based dc–dc converter system, the effectiveness of the proposed communication-free power management strategy will be verified when the input voltage, the load condition, and the droop coefficient of the ESS are changed, and when the ESU is plugged-in or plugged-out, which can be employed to simulate the potential conditions in the practice application.

#### A. Simulation Results for the Communication-Free Power Management Strategy

In this part, the Simulink model with three DAB-based dc–dc converter system is established, and the circuit parameters are illustrated in Table I.

When the droop coefficients  $k_1$ ,  $k_2$ , and  $k_3$  are 0.5, the simulation results when the input voltage  $U_{in1}$  of the first DAB module and the load resistor  $R_{TE}$  are changed can be shown in Fig. 13. As shown in Fig. 13(c), when the input voltage  $U_{in1}$  of the first DAB converter and the load condition  $R_{TE}$  are varied [see Fig. 13(a) and (b)], the corresponding transferred power can be quickly obtained by using the proposed strategy, and the transferred power of these three ESU are the same. So, as shown in Fig. 13(d), the disturbances of dc-link voltage can be neglected.

Then, when the original droop coefficients  $k_1$ ,  $k_2$ , and  $k_3$  are 0.5, the load resistor  $R_{TE}$  is 10  $\Omega$ , the input voltage  $U_{in1}$  is 60 V, the input voltage  $U_{in2}$  is 60 V, and the input voltage  $U_{in3}$  is 50 V, the simulation results when the droop coefficient  $k_1$  of the first ESU is changed between 0.5 and 1 can be illustrated in Fig. 14. As shown in Fig. 14(a), when  $k_1$  is changed, the desired dc-link voltage of the first ESU is changed suddenly. Based on the adjusting function of the PI controller and the droop controller, the new steady state of the dc-link voltage can be acquired. When  $k_1$  is increased, the new steady dc-link voltage is a little increased, and when the  $k_1$  is decreased, the new steady dc-link voltage is a little reduced. Moreover, as shown in Fig. 14(b), the power sharing performance of these three ESUs can be strictly determined by the droop coefficients according to (3).

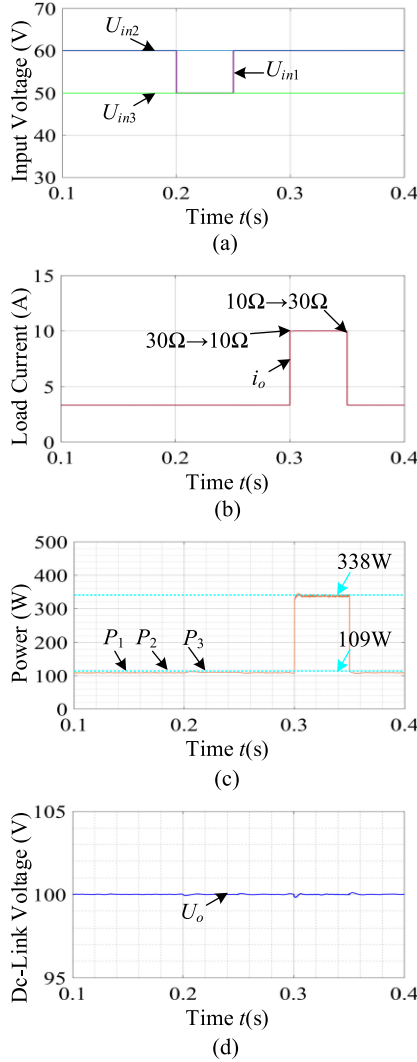


Fig. 13. Simulation results when the input voltage and load condition are changed under the proposed communication-free power management strategy. (a) Input voltages. (b) Load current. (c) Transferred powers. (d) DC-link voltage.

Moreover, when the droop coefficients  $k_1$ ,  $k_2$ , and  $k_3$  are 0.5, the load resistor  $R_{TE}$  is 30  $\Omega$ , the input voltage  $U_{in1}$  is 60 V, the input voltage  $U_{in2}$  is 60 V, and the input voltage  $U_{in3}$  is 50 V, the simulation results when the third ESU is plugged-in or plugged-out can be illustrated in Fig. 15. As shown in Fig. 15(a), based on the presented plugging-out operation, the transferred power of the third ESU can be reduced gradually, and the other ESUs can compensate the reduced power immediately. When the steady state of the multiple DAB-based converter system is obtained, the power sharing performance of these three ESUs can be strictly determined by the droop coefficients according to (3). Then, according to Fig. 15(b), the dc-link voltage can just be affected a little for achieving the steady state again. As analyze in Section III-C, when one ESU is plugged-out, the new steady dc-link voltage is a little decreased, and when one ESU is plugged-in, the new steady dc-link voltage is a little increased. In addition, as shown in Fig. 15(a), the plug-in and plug-out processes do not take a long time, and the settling time is about 0.06 ms.

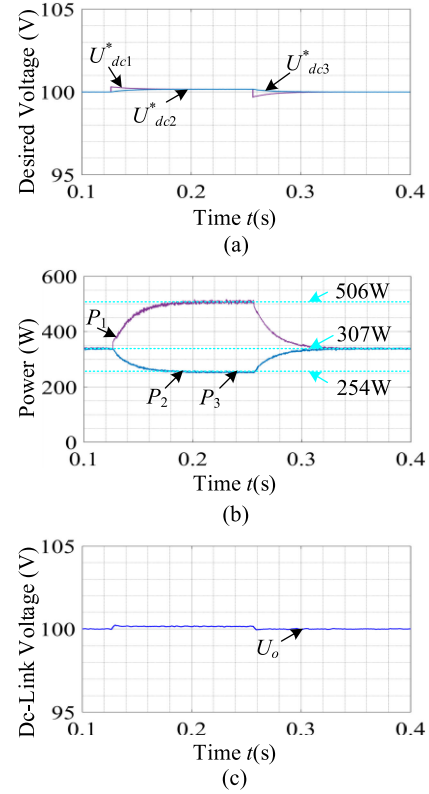


Fig. 14. Simulation results when the droop coefficient  $k_1$  of the first ESU is changed between 0.5 and 1 under the proposed communication-free power management strategy. (a) Desired voltages. (b) Transferred powers. (c) DC-link voltage.

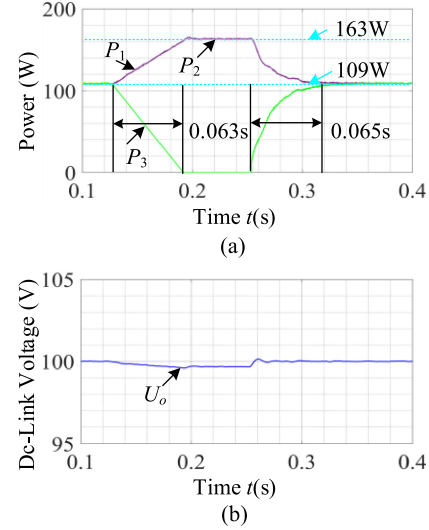


Fig. 15. Simulation results when the third ESU is plugged-in or plugged-out under the proposed communication-free power management strategy. (a) Transferred powers. (b) DC-link voltage.

Furthermore, when the third DAB is plugged-out, the detailed waveforms of the inductance current  $i_{L3}$ , the output voltage  $U_{ab3}$  of the primary-side H bridge and the output voltage  $U_{cd3}$  of the secondary-side H bridge of the third DAB converter can be shown in Fig. 16. When the switches of the third DAB module

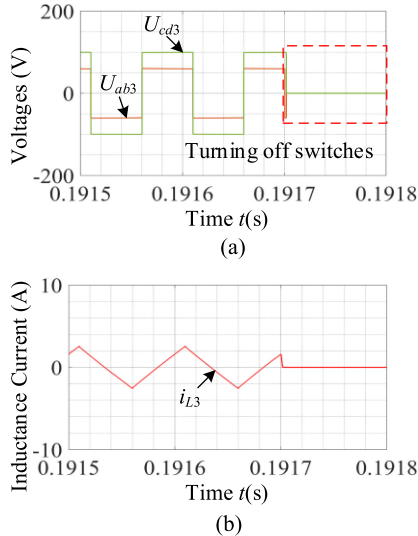


Fig. 16. Detailed waveforms of  $i_{L3}$ ,  $U_{ab3}$ , and  $U_{cd3}$  when the third ESU is plugged-out under the proposed communication-free power management strategy. (a) Voltages during plug-out process. (b) Inductance current during plug-out process.

TABLE II  
CIRCUIT PARAMETERS OF THE MULTIPLE DAB-BASED DC-DC CONVERTER SYSTEM IN EXPERIMENTAL PLATFORM

|                       |                            |
|-----------------------|----------------------------|
| Number of DAB Modules | 2                          |
| $L_1, L_2$            | 50 $\mu$ H, 80 $\mu$ H     |
| $n_1, n_2$            | 2                          |
| $f_s$                 | 10kHz                      |
| $R_{TE}$              | 16 $\Omega$ or 32 $\Omega$ |
| $U_{in1}, U_{in2}$    | 30V to 50V                 |
| $U_{nom}$             | 61V (Compensated)          |
| $U^*_{dc}$            | 60V                        |
| $k_1, k_2$            | 0 to 1                     |
| $k_{pa}, k_{ia}$      | 2.5, 0.25                  |

are turned OFF, the inductance current  $i_{L3}$  can be consumed quickly.

### B. Experiment Results for the Communication-Free Power Management Strategy

In this part, based on the dsPACE MicroLabBox, a small-scale experiment platform is established with two DAB dc-dc converters, and the experiment results are employed to verify the effectiveness of the proposed communication-free power management strategy. The circuit parameters are illustrated in Table II. The photograph of the experiment platform can be shown in Fig. 17.

When the droop coefficients  $k_1$  and  $k_2$  are 0.4, the experiment results when the input voltages  $U_{in1}$  and  $U_{in2}$  are changed between 30 and 40 V can be shown in Fig. 18. As shown in Fig. 18(a), the desired dc-link voltages  $U^*_{dc1}$  and  $U^*_{dc2}$  of the two DAB modules are not changed, and as shown in Fig. 18(b),

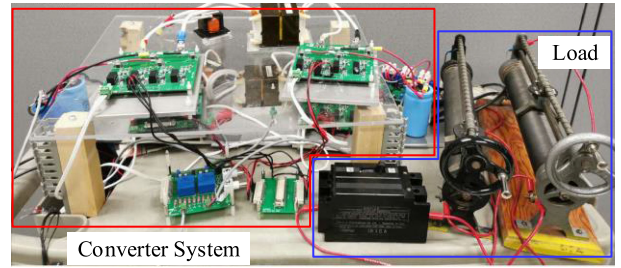


Fig. 17. Photograph of the experiment platform.

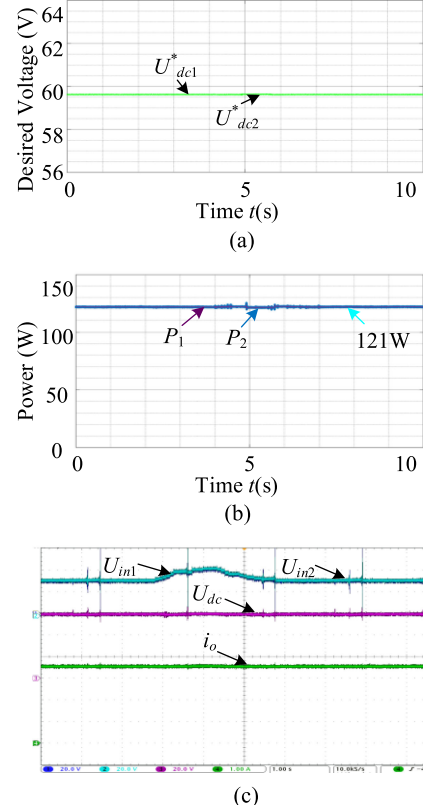


Fig. 18. Experiment results when the input voltage is changed under the proposed communication-free power management strategy ( $U_{in1}$  and  $U_{in2}$ : 20 V/div;  $U_{dc}$ : 20 V/div;  $i_o$ : 2 A; and  $t$ : 1 s/div). (a) Desired dc-link voltages. (b) Transferred powers. (c) Measured voltages and currents.

the transferred powers  $P_1$  and  $P_2$  of these two DAB modules are stable during the input-voltage change process. Then, when the input voltages  $U_{in1}$  and  $U_{in2}$  are changed between 30 and 40 V, the dc-link voltage  $U_{dc}$  can be maintained at its desired value 60 V [see Fig. 18(c)]. Therefore, based on the proposed communication-free power management strategy, the excellent dynamic performance can be provided for the multiple DAB-based ESS when the output voltage of the energy storage equipment is changed.

Then, when the droop coefficients  $k_1$  and  $k_2$  are 0.4, and the input voltages  $U_{in1}$  and  $U_{in2}$  are 30 V, the experiment results when the load resistor  $R_{TE}$  is changed between 16 and 32  $\Omega$  can be shown in Fig. 19. As shown in Fig. 19(a), the

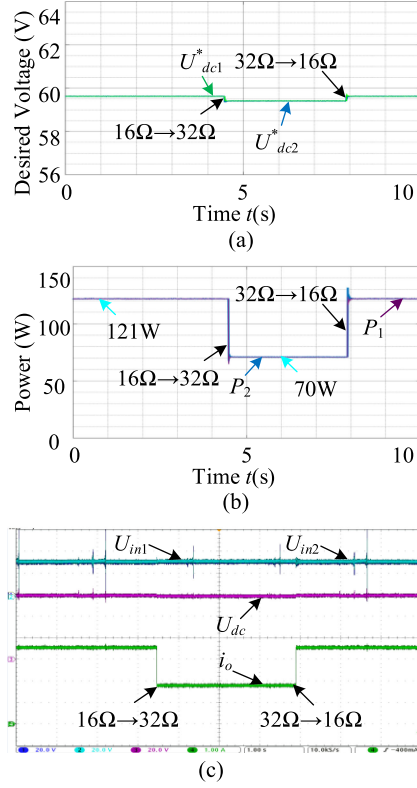


Fig. 19. Experiment results when the load condition is changed under the proposed communication-free power management strategy ( $U_{in1}$  and  $U_{in2}$ : 20 V/div;  $U_{dc}$ : 20 V/div;  $i_o$ : 2 A; and  $t$ : 1 s/div). (a) Desired dc-link voltages. (b) Transferred powers. (c) Measured voltages and currents.

desired dc-link voltages  $U^*_{dc1}$  and  $U^*_{dc2}$  of these two DAB modules have a few disturbances when the load resistor  $R_{TE}$  are changed, which may be affected by the power loss of the converter system. When the converter system is working at light-load condition, the efficiency is preferred to be low, which means more transferred power should be provided to balance the relationship between the output power and the transferred power. Then, according to (3), the desired dc-link voltage will be reduced a little at light-load condition. Moreover, when the load resistor  $R_{TE}$  is suddenly changed, the corresponding transferred power can be quickly provided by using the proposed communication-free power management strategy. Furthermore, as shown in Fig. 19(c), when the load resistor  $R_{TE}$  is changed between 16 and 32 Ω, the dc-link voltage can remain at its desired value, and the disturbances of the dc-link voltage can be omitted. Thus, when the load condition is changed, the fast responses can be provided for the multiple DAB-based ESS by using the communication-free power management strategy.

Moreover, when the original droop coefficients  $k_1$  and  $k_2$  are 0.4, the input voltages  $U_{in1}$  and  $U_{in2}$  are 30 V and the load resistor  $R_{TE}$  is 32 Ω, the experiment results when the droop coefficient  $k_2$  of the second DAB module is changed between 0.4 and 0.2 can be illustrated in Fig. 20. As shown in Fig. 20(a), the desired dc-link voltages  $U^*_{dc1}$  and  $U^*_{dc2}$  of these two DAB modules have a few disturbances when the droop coefficient  $k_2$  is changed. When  $k_2$  is changed, the desired dc-link voltage

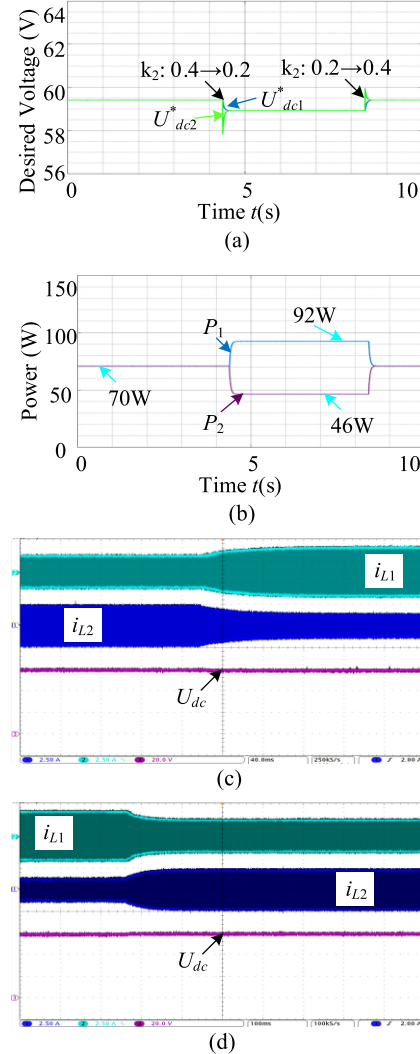


Fig. 20. Experiment results when the droop coefficient  $k_2$  of the second ESU is changed between 0.4 and 0.2 under the proposed communication-free power management strategy ( $i_{L1}$  and  $i_{L2}$ : 2.5 A/div;  $U_{dc}$ : 20 V/div; and  $t$ : 100 ms/div). (a) Desired dc-link voltages. (b) Transferred powers. (c)  $k_2$ : 0.4→0.2. (d)  $k_2$ : 0.2→0.4.

$U^*_{dc2}$  of the second ESU is changed suddenly. Based on the adjusting function of the droop control structure, the new steady state of the dc-link voltage can be acquired. According to (3), when  $k_2$  is increased, the new steady dc-link voltage is a little increased, and when  $k_2$  is decreased, the new steady dc-link voltage is a little reduced. Moreover, when the droop coefficient  $k_2$  is changed between 0.4 and 0.2, the transferred powers  $P_1$  and  $P_2$  are changed gradually to reach the steady state again. Furthermore, as shown in Fig. 20(c) and (d), when the droop coefficient  $k_2$  is changed between 0.2 and 0.4, the dc-link voltage can remain at its desired value, and the disturbances of the dc-link voltage can be omitted. Thus, when the droop coefficient is changed for different power sharing performance, the fast responses can be provided for the multiple DAB-based ESS by using the communication-free power management strategy.

In addition, when the original droop coefficients  $k_1$  and  $k_2$  are 0.4, the input voltages  $U_{in1}$  and  $U_{in2}$  are 30 V and the load

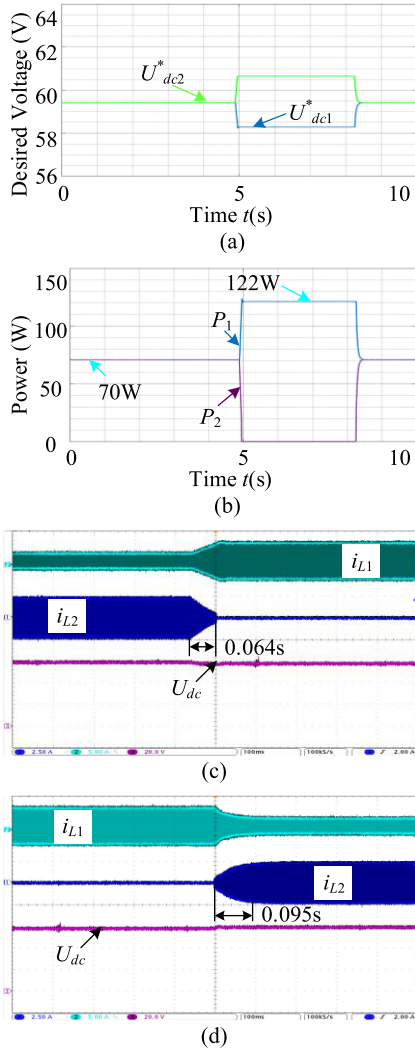


Fig. 21. Experiment results when the second ESU is plugged-out or plugged-in under the proposed communication-free power management strategy ( $i_{L1}$ : 5 A/div;  $i_{L2}$ : 2.5 A/div;  $U_{dc}$ : 20 V/div; and  $t$ : 100 ms/div). (a) Desired dc-link voltages. (b) Transferred powers. (c) Plug-out process. (d) Plug-in process.

resistor  $R_{TE}$  is  $32 \Omega$ , the experiment results when the second DAB converter is plugged-out and plugged-in can be illustrated in Fig. 21. As shown in Fig. 21(a), when the second DAB module is plugged-out, the desired dc-link voltage  $U_{dc2}^*$  is a little reduced, and when the second DAB module is plugged-in, the desired dc-link voltage  $U_{dc1}^*$  is a little increased since the desired dc-link voltage is affected by the DAB number, as demonstrated in (13). Moreover, as shown in Fig. 21(b), the transferred powers  $P_1$  and  $P_2$  are changed gradually to reach the steady state again during the plug-out and plug-in processes. Furthermore, as shown in Fig. 21(c) and (d), when the second DAB converter is plugged-out or plugged-in, the dc-link voltage  $U_{dc}$  is always close to its expected value 60 V, and the settling time is smaller than 0.1 s. Thus, based on the communication-free power management strategy, the robustness of the dc-link voltage can be ensured when the ESU is plugged-out or plugged-in, and the plug-in and plug-out processes do not take a long time.

#### IV. CONCLUSION

In this article, a communication-free power management strategy with seamless hot swap ability is proposed, which can combine the droop control concept, the dynamic optimization control, and the all kinds of phase-shift modulation methods for the multiple DAB-based ESS. Based on simulation and experimental verifications of the proposed strategy, the conducted studies in this article can lead to the following conclusions.

- 1) Based on the proposed communication-free power management strategy, the dc-link voltage can be kept stable when the output voltage of the energy storage equipment and the load condition of the multiple DAB-based converter system are changed, and excellent dynamic performance can be obtained.
- 2) Based on the proposed communication-free power management strategy, when the droop coefficient is changed for different SOC of the energy storage equipment, the dc-link voltage can be maintained at its desired value.
- 3) Based on the presented plug-in and plug-out operation for the ESU, the new ESU can be directly plugged-in for increasing the power capacity of the ESS without reprogramming operation and influencing the dc-link voltage, and the ESU can also be plugged-out without obvious impact on the dc-link voltage.
- 4) Combining some existing SOC balancing methods, the balanced state of change performance of the ESS can be obtained under the proposed communication-free power management strategy. Furthermore, when the centralized man-machine interaction system is required for better control performance of the ESS, the proposed scheme is easily extended to high-level management system.

#### REFERENCES

- [1] B. Liu, F. Zhuo, Y. Zhu, and H. Yi, "System operation and energy management of a renewable energy-based DC micro-grid for high penetration depth application," *IEEE Trans. Smart Grid*, vol. 6, no. 3, pp. 1147–1155, May 2015.
- [2] Y. Li, D. M. Vilathgamuwa, and P. C. Loh, "Design, analysis, and real-time testing of a controller for multibus microgrid system," *IEEE Trans. Power Electron.*, vol. 19, no. 5, pp. 1195–1204, Sep. 2004.
- [3] X. Li, L. Guo, C. Hong, Y. Zhang, Y. W. Li, and C. Wang, "Hierarchical control of multiterminal DC grids for large-scale renewable energy integration," *IEEE Trans. Sustain. Energy*, vol. 9, no. 3, pp. 1448–1457, Jul. 2018.
- [4] N. L. Díaz, A. C. Luna, J. C. Vasquez, and J. M. Guerrero, "Centralized control architecture for coordination of distributed renewable generation and energy storage in islanded AC microgrids," *IEEE Trans. Power Electron.*, vol. 32, no. 7, pp. 5202–5213, Jul. 2017.
- [5] T. Kovaltchouk, A. Blavette, J. Aubry, H. B. Ahmed, and B. Multon, "Comparison between centralized and decentralized storage energy management for direct wave energy converter farm," *IEEE Trans. Energy Convers.*, vol. 31, no. 3, pp. 1051–1058, Sep. 2016.
- [6] P. Karlsson and J. Svensson, "DC bus voltage control for a distributed power system," *IEEE Trans. Power Electron.*, vol. 18, no. 6, pp. 1405–1412, Nov. 2003.
- [7] K. Sun, L. Zhang, Y. Xing, and J. M. Guerrero, "A distributed control strategy based on DC bus signaling for modular photovoltaic generation systems with battery energy storage," *IEEE Trans. Power Electron.*, vol. 26, no. 10, pp. 3032–3045, Oct. 2011.
- [8] N. Hou and Y. W. Li, "A tunable power sharing control scheme for the output-series DAB DC-DC system with independent or common input terminals," *IEEE Trans. Power Electron.*, vol. 34, no. 10, pp. 9386–9391, Oct. 2019.

- [9] X. Shen, M. Shahidehpour, Y. Han, S. Zhu, and J. Zheng, "Expansion planning of active distribution networks with centralized and distributed energy storage systems," *IEEE Trans. Sustain. Energy*, vol. 8, no. 1, pp. 126–134, Jan. 2017.
- [10] J. Xiao, P. Wang, and L. Setyawati, "Hierarchical control of hybrid energy storage system in DC microgrids," *IEEE Trans. Ind. Electron.*, vol. 62, no. 8, pp. 4915–4924, Aug. 2015.
- [11] C. Yuan, M. A. Haj-ahmed, and M. S. Illindala, "Protection strategies for medium-voltage direct-current microgrid at a remote area mine site," *IEEE Trans. Ind. Appl.*, vol. 51, no. 4, pp. 2846–2853, Jul./Aug. 2015.
- [12] M. B. Shadmand and R. S. Balog, "Multi-objective optimization and design of photovoltaic-wind hybrid system for community smart DC microgrid," *IEEE Trans. Smart Grid*, vol. 5, no. 5, pp. 2635–2643, Sep. 2014.
- [13] P. García, P. Arboleya, B. Mohamed, and A. A. C. Vega, "Implementation of a hybrid distributed/centralized real-time monitoring system for a DC/AC microgrid with energy storage capabilities," *IEEE Trans. Ind. Informat.*, vol. 12, no. 5, pp. 1900–1909, Oct. 2016.
- [14] A. Agrawal, C. S. Nalamati, and R. Gupta, "Hybrid DC–AC zonal microgrid enabled by solid-state transformer and centralized ESD integration," *IEEE Trans. Ind. Electron.*, vol. 66, no. 11, pp. 9097–9107, Nov. 2019.
- [15] J. Xiao, P. Wang, and L. Setyawati, "Multilevel energy management system for hybridization of energy storages in DC microgrids," *IEEE Trans. Smart Grid*, vol. 7, no. 2, pp. 847–856, Mar. 2016.
- [16] T. R. Oliveira, W. W. A. Gonçalves Silva, and P. F. Donoso-Garcia, "Distributed secondary level control for energy storage management in DC microgrids," *IEEE Trans. Smart Grid*, vol. 8, no. 6, pp. 2597–2607, Nov. 2017.
- [17] Y. Xia, M. Yu, P. Yang, Y. Peng, and W. Wei, "Generation-storage coordination for islanded DC microgrids dominated by PV generators," *IEEE Trans. Energy Convers.*, vol. 34, no. 1, pp. 130–138, Mar. 2019.
- [18] R. W. A. A. De Doncker, D. M. Divan, and M. H. Kheraluwala, "A three-phase soft-switched high-power-density DC/DC converter for high-power applications," *IEEE Trans. Ind. Appl.*, vol. 27, no. 1, pp. 63–73, Jan./Feb. 1991.
- [19] B. Zhao, Q. Song, W. Liu, and Y. Sun, "Overview of dual-active-bridge isolated bidirectional DC–DC converter for high-frequency-link power-conversion system," *IEEE Trans. Power Electron.*, vol. 29, no. 8, pp. 4091–4106, Aug. 2014.
- [20] N. Hou and Y. W. Li, "Overview and comparison of modulation and control strategies for a nonresonant single-phase dual-active-bridge DC–DC converter," *IEEE Trans. Power Electron.*, vol. 35, no. 3, pp. 3148–3172, Mar. 2020.
- [21] F. An, W. Song, K. Yang, N. Hou, and J. Ma, "Improved dynamic performance of dual active bridge DC–DC converters using MPC scheme," *IET Power Electron.*, vol. 11, no. 11, pp. 1756–1765, 2018.
- [22] W. Song, N. Hou, and M. Wu, "Virtual direct power control scheme of dual active bridge DC–DC converters for fast dynamic response," *IEEE Trans. Power Electron.*, vol. 33, no. 2, pp. 1750–1759, Feb. 2018.
- [23] G. G. Oggier, M. Ordóñez, J. M. Galvez, and F. Luchino, "Fast transient boundary control and steady-state operation of the dual active bridge converter using the natural switching surface," *IEEE Trans. Power Electron.*, vol. 29, no. 2, pp. 946–957, Feb. 2014.
- [24] F. An, W. Song, B. Yu, and K. Yang, "Model predictive control with power self-balancing of the output parallel DAB DC–DC converters in power electronic traction transformer," *IEEE J. Emerg. Sel. Topics Power Electron.*, vol. 6, no. 4, pp. 1806–1818, Dec. 2018.
- [25] N. Hou and Y. Li, "The comprehensive circuit-parameter estimating strategies for output-parallel dual-active-bridge DC–DC converters with tunable power sharing control," *IEEE Trans. Ind. Electron.*, vol. 67, no. 9, pp. 7583–7594, Sep. 2020.
- [26] J. Liu, J. Yang, J. Zhang, Z. Nan, and Q. Zheng, "Voltage balance control based on dual active bridge DC/DC converters in a power electronic traction transformer," *IEEE Trans. Power Electron.*, vol. 33, no. 2, pp. 1696–1714, Feb. 2018.
- [27] R. Majumder, B. Chaudhuri, A. Ghosh, R. Majumder, G. Ledwich, and F. Zare, "Improvement of stability and load sharing in an autonomous microgrid using supplementary droop control loop," *IEEE Trans. Power Syst.*, vol. 25, no. 2, pp. 796–808, May 2010.
- [28] X. Li *et al.*, "Observer-based DC voltage droop and current feed-forward control of a DC microgrid," *IEEE Trans. Smart Grid*, vol. 9, no. 5, pp. 5207–5216, Sep. 2018.
- [29] K. D. Hoang and H. Lee, "Accurate power sharing with balanced battery state of charge in distributed DC microgrid," *IEEE Trans. Ind. Electron.*, vol. 66, no. 3, pp. 1883–1893, Mar. 2019.
- [30] X. Lu, J. M. Guerrero, K. Sun, and J. C. Vasquez, "An improved droop control method for DC microgrids based on low bandwidth communication with DC bus voltage restoration and enhanced current sharing accuracy," *IEEE Trans. Power Electron.*, vol. 29, no. 4, pp. 1800–1812, Apr. 2014.
- [31] H. Bai and C. Mi, "Eliminate reactive power and increase system efficiency of isolated bidirectional dual-active-bridge DC–DC converters using novel dual-phase-shift control," *IEEE Trans. Power Electron.*, vol. 23, no. 6, pp. 2905–2914, Nov. 2008.
- [32] B. Zhao, Q. Yu, and W. Sun, "Extended-phase-shift control of isolated bidirectional DC–DC converter for power distribution in microgrid," *IEEE Trans. Power Electron.*, vol. 27, no. 11, pp. 4667–4680, Nov. 2012.
- [33] G. Oggier, G. O. García, and A. R. Oliva, "Modulation strategy to operate the dual active bridge DC–DC converter under soft switching in the whole operating range," *IEEE Trans. Power Electron.*, vol. 26, no. 4, pp. 1228–1236, Apr. 2011.
- [34] N. Hou, W. Song, and M. Wu, "Minimum-current-stress scheme of dual active bridge DC–DC converter with unified phase-shift control," *IEEE Trans. Power Electron.*, vol. 31, no. 12, pp. 8552–8561, Dec. 2016.
- [35] A. Tong, L. Hang, G. Li, X. Jiang, and S. Gao, "Modeling and analysis of a dual-active-bridge-isolated bidirectional DC/DC converter to minimize RMS current with whole operating range," *IEEE Trans. Power Electron.*, vol. 33, no. 6, pp. 5302–5316, Jun. 2018.
- [36] X. Lu, K. Sun, J. M. Guerrero, J. C. Vasquez, and L. Huang, "Double-quadrant state-of-charge-based droop control method for distributed energy storage systems in autonomous DC microgrids," *IEEE Trans. Smart Grid*, vol. 6, no. 1, pp. 147–157, Jan. 2015.
- [37] X. Lu, K. Sun, J. M. Guerrero, J. C. Vasquez, and L. Huang, "State-of-charge balance using adaptive droop control for distributed energy storage systems in DC microgrid applications," *IEEE Trans. Ind. Electron.*, vol. 61, no. 6, pp. 2804–2815, Jun. 2014.



**Nie Hou** (Student Member, IEEE) received the B.S. and M.S. degrees in electrical engineering from Southwest Jiaotong University, Chengdu, China, in 2014 and 2017, respectively. He is currently working toward the Ph.D. degree with the Department of Electrical and Computer Engineering, University of Alberta, Edmonton, AB, Canada.

His current research interests include digital control and optimization methods of dc–dc converter and dc distribution system.

Mr. Hou was the recipient of the Outstanding Author Award from the Proceeding of the Chinese Society for Electrical Engineering in 2016.



**Yunwei Li** (Fellow, IEEE) received the B.Sc. degree in electrical engineering from Tianjin University, Tianjin, China, in 2002, and the Ph.D. degree from Nanyang Technological University, Singapore, in 2006.

In 2005, he was a Visiting Scholar with Aalborg University, Aalborg, Denmark. From 2006 to 2007, he was a Postdoctoral Research Fellow with Ryerson University, Toronto, ON, Canada. In 2007, he was with Rockwell Automation Canada. In 2007, he also joined the University of Alberta, Edmonton, AB, Canada, where he is currently a Professor. His research interests include distributed generation, microgrid, renewable energy, high-power converters, and electric motor drives.

Dr. Li serves as an Editor-in-Chief for the IEEE TRANSACTIONS ON POWER ELECTRONICS LETTERS. Prior to that, he was an Associate Editor for the IEEE TRANSACTIONS ON POWER ELECTRONICS, IEEE TRANSACTIONS ON INDUSTRIAL ELECTRONICS, IEEE TRANSACTIONS ON SMART GRID, and IEEE JOURNAL OF EMERGING AND SELECTED TOPICS IN POWER ELECTRONICS. He was the recipient of the Richard M. Bass Outstanding Young Power Electronics Engineer Award from the IEEE Power Electronics Society in 2013 and the Second Prize Paper Award of the IEEE TRANSACTIONS ON POWER ELECTRONICS in 2014.